RESEARCH PAPER

Quenching of High Entropy Alloys after Annealing

E. Abbasi[1*], K. Dehghani[1], S. V. Sajadifar[2] and T. Niendorf[2]

** engabasi@gmail.com*

Received: May 2020 Revised: August 2020 Accepted: October 2020

[1] Department of Materials and Metallurgical Engineering, Amirkabir University of Technology, Tehran, Iran
[2] Universität Kassel, Institut Für Werkstofftechnik (Materials Engineering), Kassel, Germany

DOI: 10.22068/ijmse.17.4.130

Abstract: *The effect of cooling rate after annealing at 900 °C on the microstructure and hardness of high entropy alloys was investigated using two typical samples with the chemical composition of $Co_{16}Cr_{14.5}Fe_{29}Mn_{11.5}Ni_{29}$ and $Co_{11.5}Cr_7Fe_{27}Mn_{27}Ni_{27}(Nb_{0.08}C_{0.5})$ (at%). The microstructural characterisation and hardness measurements were carried out by optical microscopy, scanning electron microscopy, wavelength-dispersive X-ray spectroscopy, electron back scattered diffraction, X-ray diffraction technique and Vickers hardness testing. A face centred cubic crystal structure matrix was observed in both alloys before and after annealing and regardless of cooling conditions. SEM analyses revealed an extensive precipitation in $Co_{11.5}Cr_7Fe_{27}Mn_{27}Ni_{27}$ ($Nb_{0.08}C_{0.5}$) alloy after annealing. It was also found that air/furnace cooling can enhance grain growth-coarsening just in $Co_{16}Cr_{14.5}Fe_{29}Mn_{11.5}Ni_{29}$. However, the hardness results generally showed insignificant hardness variations in both alloys after water-quenching, air-cooling and furnace-cooling. The results suggested that the hardness is mainly controlled by solid solution strengthening.*

Keywords: *High entropy alloys, Cooling rate, Annealing, Microstructure, Hardness.*

1. INTRODUCTION

Since 2004, High entropy Alloys (HEA) as one group of advanced materials have attracted much attention due to their outstanding mechanical properties at cryogenic, room and high temperatures [1-3]. HEAs have shown excellent hot and cryogenic strengths and ductility, high fracture toughness, remarkable wear and corrosion resistance etc. Hence, HEAs are considered as promising candidates for substitution of stainless steels, superalloys and bulk metallic glass (BMG), where severe loading and thermal conditions are applied.

In this context, Compositionally Complex Alloys (CCA) concept has been driven by the HEA approach in order to manipulate a microstructure consisting of a high entropy matrix in addition to secondary phases [4-6]. This has been achieved by controlling processing parameters and chemical composition of HEAs [4, 7]. It has been well understood that the CCAs can give a better mechanical and physical properties compared to HEAs due to their complex microstructure. However, further investigations into the processing and chemical composition of CCAs/HEAs are still sought.

The chemical composition of HEAs/CCAs is designed by taking into consideration of different empirical and thermodynamic principals, e.g. entropy of mixing, enthalpy of mixing, atomic size difference and valence electron concentration [2, 5]. So far, many investigations have been done on these principals and it has been shown that they must be within certain range in order to guarantee a stable high entropy solid solution [8, 9]. It has been established that the solid solution matrix of HEAs is considerably stable during thermomechanical processing and also against mechanical deformation [10]. This can secure the stability of mechanical properties and microstructure.

Thermomechanical processing parameters of different alloys have been well studied and they are used to design manufacturing processes [11, 12]. In this way, just a few investigations have been reported on the effect of cooling conditions on the microstructure and mechanical properties of HEAs/CCAs after casting and heat treatments [13-16]. In general, they showed that the cooling rate can effectively influence the microstructural evolution of HEAs, though there is still lack of discussion on cooling rate during annealing. Also, several researchers have shown the possibility of precipitation in HEAs/CCAs below their solidus during aging/annealing [17-19, 6]. Thus, the question arises: to what extent can the

[DOI: 10.22068/ijmse.17.4.130]

cooling rate change the microstructure of HEAs during annealing. However, this question has not clearly been answered in the literature.

In this study, two non-equiatomic HEAs with different chemical compositions were chosen based on our previous theoretical and experimental analyses [8]. It was believed that the chosen chemical compositions for the studied alloys can provide a Face Centred Cubic (FCC) matrix during solidification, whereas precipitation behaviour can be different between two alloys. Concurrent investigations into the effect of Nb-C addition in CoCrFeMnNi HEA have shown remarkable precipitation in cold rolled condition during annealing in this alloy system [20]. Other researchers also have reported that CoCrFeMnNi HEA is strongly stable and precipitation can only occur in its microstructure after prolonged exposure at high temperatures and also once non-equiatomic compositions are used [21-23]. The studied HEAs had been homogenised at a relatively high temperature for 24 h before annealing. This would have provided a homogenous microstructure, consisting of a low level of crystalline defects and with dissolved precipitates that could minimise possible precipitation on crystalline defects and recrystallisation during subsequent annealing [24, 8]. Therefore, the main aim of this investigation was to understand the effect of cooling rate on the stability of microstructure and hardness of such alloy systems after annealing.

2. EXPERIMENTAL PROCEDURE

The studied alloys were two non-equiatomic HEAs and were melted from pure metals (purity > 99.8 wt.%) in a centrifugal Vacuum Induction Melting furnace (VIM - Linn Platicast 600). The ingots (10x20x80 mm^3) were homogenised at 1200 ˚C for 24 h in argon atmosphere, followed by rapid air cooling, to breakdown the dendritic structure and to increase the homogeneity of alloying elements.

The cooling conditions was simulated by three-dimensional non-linear Finite Element (FE) method using Abaqus (coupled temperature-displacement) commercial software (Dassault Systèmes, Providence, Rhode Island) to evaluate thermal stress and temperature distribution throughout sample. Isotropic properties were employed from the available data in the literature [25-28] and also air/water cooling conditions were applied for the FE simulations.

The chemical composition of each alloy was determined from the cross-sectional area of the ingot by a Philips X Unique II XRF machine and Leco-combustion technique (Table 1). It should be noted that the standard deviation of XRF technique for principal elements was ±0.2 wt% and for minor element was ±0.004 wt% hence the results were rounded off to avoid any confusion. Furthermore, entropy of mixing (ΔS_{mix}) was calculated using the following equation:

$$\Delta S_{mix} = -R\sum_{i=1}^{n} C_i \mathrm{Ln} C_i \quad (1)$$

Where, C_i is the atomic fraction of elements i. The calculated ΔS_{mix} for the studied alloys showed that both studied alloys can be solid solution high entropy alloys (Table 1).

Samples with a thickness of 5 mm were cut from the cross-sectional area of ingot and subjected to annealing at 900 ˚C for 1 h before cooling at different rates to room temperature (Fig. 1). The annealing temperature was chosen based on our previous investigations by JMatPro simulations [24, 8]. From simulation analysis, it is believed that just gamma phase and also carbides could exist at this temperature. The temperature of specimen was measured by a k-type thermocouple, attached to the middle section of specimen. Subsequently, the average cooling rate was calculated from the recorded data.

Table 1. Chemical composition of studied alloys (at.%)

Material	Co	Cr	Fe	Mn	Ni	Nb	C	ΔSmix (J $mol^{-1}K^{-1}$)
Alloy 1	16.00	14.50	29.00	11.50	29.00	-	-	12.8
Alloy 2	11.50	7.00	27.00	27.00	27.00	0.08	0.50	12.7

[DOI: 10.22068/ijmse.17.4.130]

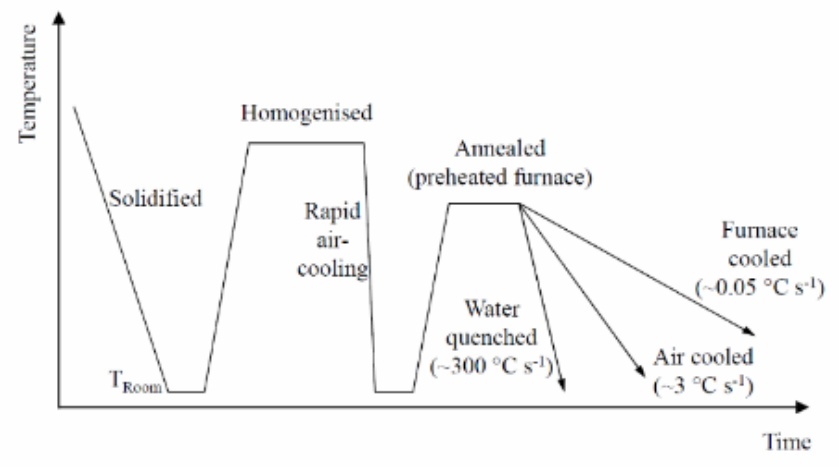

Fig. 1. The heat treatment schedule used to prepare samples.

Microstructural characterisations and hardness measurements were carried out using homogenised and annealed samples [29]. Microstructure was examined through optical microscopy, Scanning Electron Microscopy (SEM) and qualitative Wavelength-dispersive X-ray spectroscopy (WDX), and X-Ray Diffraction (XRD) techniques. Samples were etched in the Marble agent (50 mL H_2O, 10 g $CuSO_4$, 50 mL HCl). SEM analyses were done by a Philips XL 30 at 25 kV. Electron Back Scattered Diffraction (EBSD) technique with a step size of 2 µm was used to study the effect of cooling rate on the sub-structure formation of studied CCAs. EBSD samples were polished by 40 µm colloidal silica suspension. Grain size was measured based on the linear intercept method by Buehler Omnimet version 9.5 in compliance with ASTM E112.

The crystalline structure of studied alloys was characterised by XRD technique using an X'Pert-Pro MPD (PANalytical) X-ray diffractometer with Cu Kα radiation at 40 kV and 40 mA. XRD spectrum was obtained from 20 to 100 degree at a step size of 0.02 degree. Quantitative analysis of XRD results was performed by Rietveld refinement method using the Topas academic package software V5.0. From the XRD results the average dislocation density of all samples was approximated according to the Williamson–Hall (WH) method using the following relation [30]. To minimise the possible effect of residual stresses on the surface due to sample preparation, samples were etched after polishing and subsequently polished again.

$$\text{Dislocation density} = 14.4(\varepsilon^2/b^2) \quad (1)$$

Where, ε and b are microstrain and Burger's vector ($b=\sqrt{2}/2$*lattice constant=0.255 nm for FCC [31, 32]), respectively. The ε was calculated using the following equation.

$$\alpha+2\varepsilon(\sin\theta/\lambda)=\delta(\cos\theta/\lambda) \quad (2)$$

$$\alpha=0.9/D \quad (3)$$

Where, θ, λ, δ and D are diffraction angle (radians), X-ray wavelength, the Full Width Half Maximum (FWHM)) and average particle size, respectively.

A Koopa UV1 Vickers hardness tester with 30 kgf load and 10 s holding time before unloading was used to measure the hardness of studied alloys according to ASTM E92. Average hardness was calculated from ten measurements per each sample.

3. RESULTS

Fig. 2 shows the distribution of stress and temperature through the sample during air cooling. It was clear that the surface was initially cooled and the temperature was gradually reduced toward the centre of sample. Moreover, the results suggested the possible stress concentration at central region of cubic shaped sample. These results agree with other reports in literature [33-35], suggesting a possible temperature and stress concentration in the sample that might affect the microstructural evolution during subsequent heat treatments.

[DOI: 10.22068/ijmse.17.4.130]

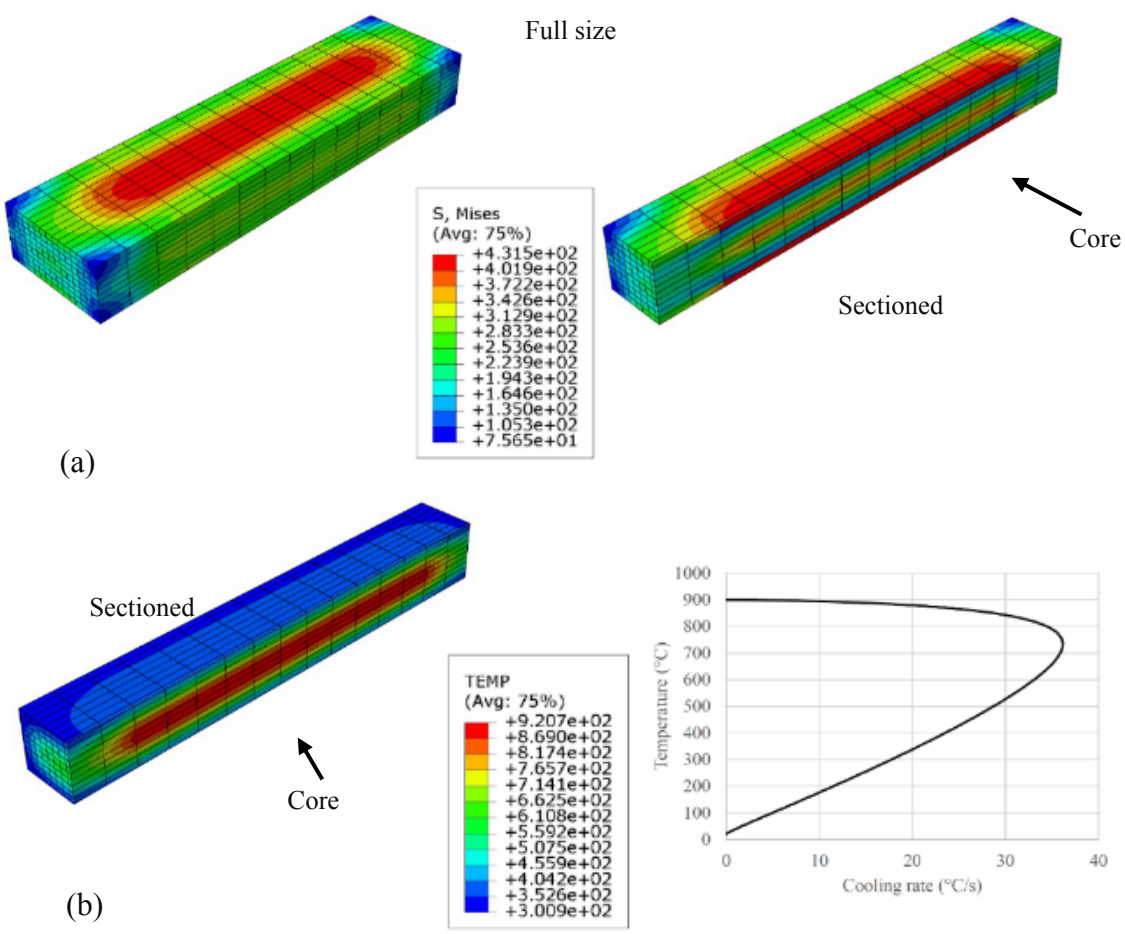

Fig. 2. Abaqus simulation of rapid air-cooling from 900 °C, (a) Stress concentration during cooling stage, (b) Temperature gradient and relevant cooling rate versus temperature.

3.1. Microstructure

Visual inspections of samples suggested the absence of any quenching defects in the studied samples. On the other hand, FEM analysis suggested a possible stress concentration at the centre of sample that could form quenching defects inside the sample during quenching (Fig. 2). This will be further clarified in the next section.

Fig. 3 shows the microstructure of studied alloys before and after annealing. The results indicated that the microstructure of homogenised samples (i.e. before annealing) was comprised of large polygonal grains with a grain size of over 100 µm in both alloys. Microscopy observations also revealed porosities inside the microstructure of both alloys.

Figs. 3 (c) to (h) highlight the effect of cooling rate on the microstructure of studied alloys. Clearly, no recrystallisation occurred in Alloy 2, while recrystallisation appeared in Alloy 1 (37.1±6.4 and 25.6±3.1 µm are the grain size of recrystallised grains in air cooled and water quenched samples, respectively). It should be mentioned that the recrystallisation mainly happened at very small regions of sample (i.e. near the centre of cross-sectional area of cast ingot) and grains were relatively larger at regions near the surface (Fig. 4). Moreover, annealing twins were observed in the recrystallised region of samples.

Fig. 5 shows EBSD Inverse Pole Figure (IPF) maps of studied CCAs in terms of cooling rate. Note that low angle boundaries (i.e. 2-15 degree) were marked by white lines, whereas high angle boundaries (i.e. >15 degree) were marked by black lines. In water quenched samples, the results indicated the presence of polygonal sub-structure inside coarse grains with high angle grain boundaries. These results are in line with optical microscopy analyses (Fig. 3) and showed that the observed sub-structure seems to be

[DOI: 10.22068/ijmse.17.4.130]

disappearing during air cooling. EBSD results also suggested that the observed sub-structure was completely disappeared in furnace cooled samples of both CCAs.

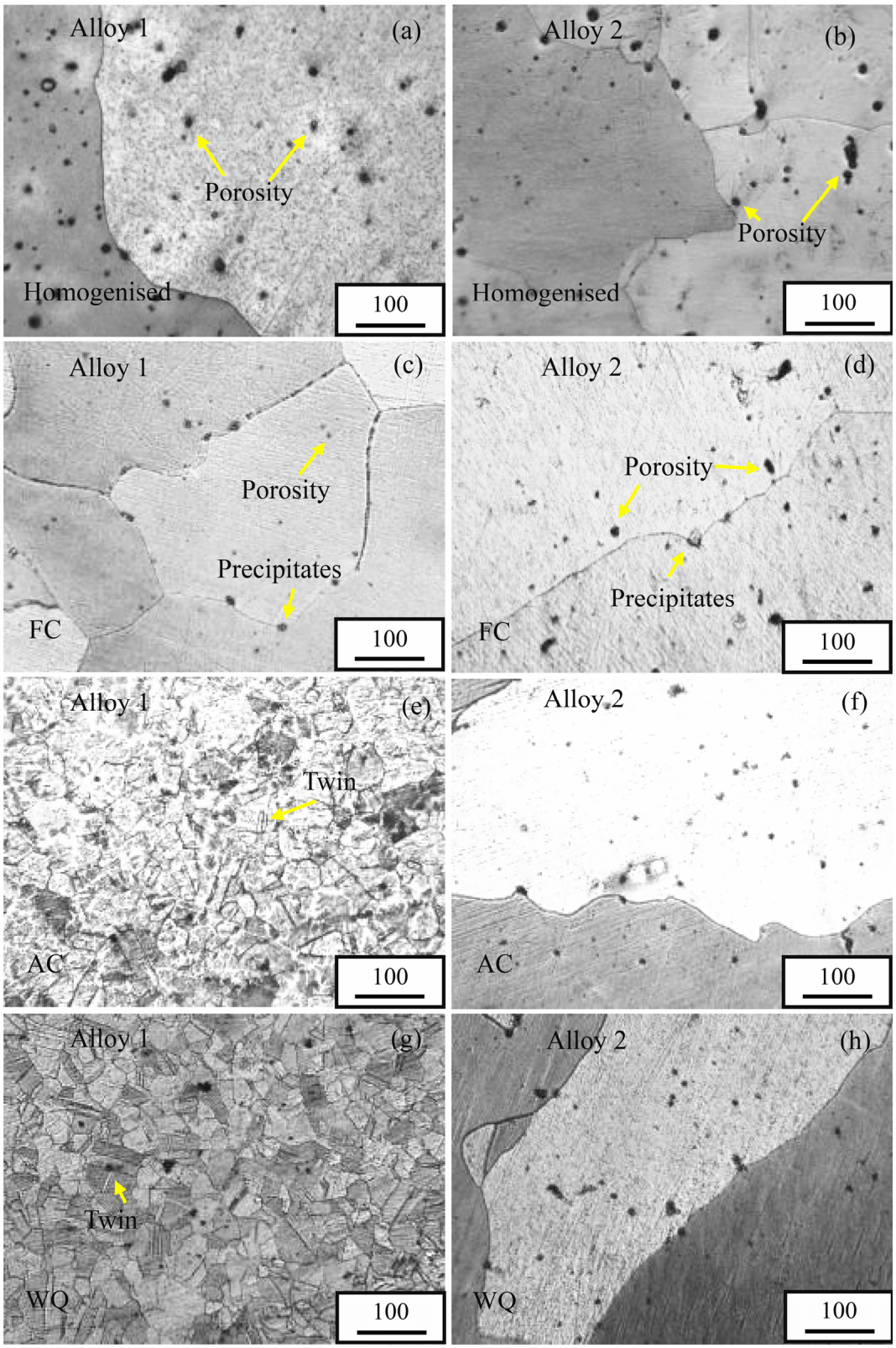

Fig. 3. Optical micrographs of studied alloys, before and after annealing, FC; furnace cooled, AC; air cooled, WQ; water quenched.

[DOI: 10.22068/ijmse.17.4.130]

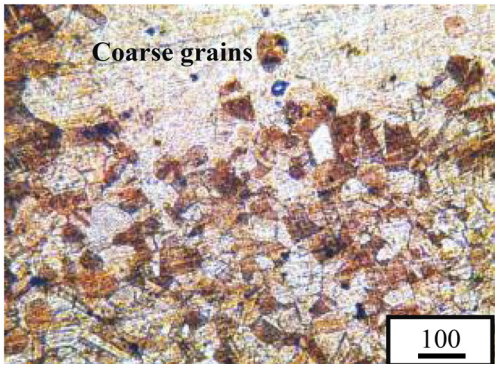

Fig. 4. Optical micrograph of Alloy 1 after air cooling, showing the recrystallised structure at the centre of sample and coarse grains near the surface.

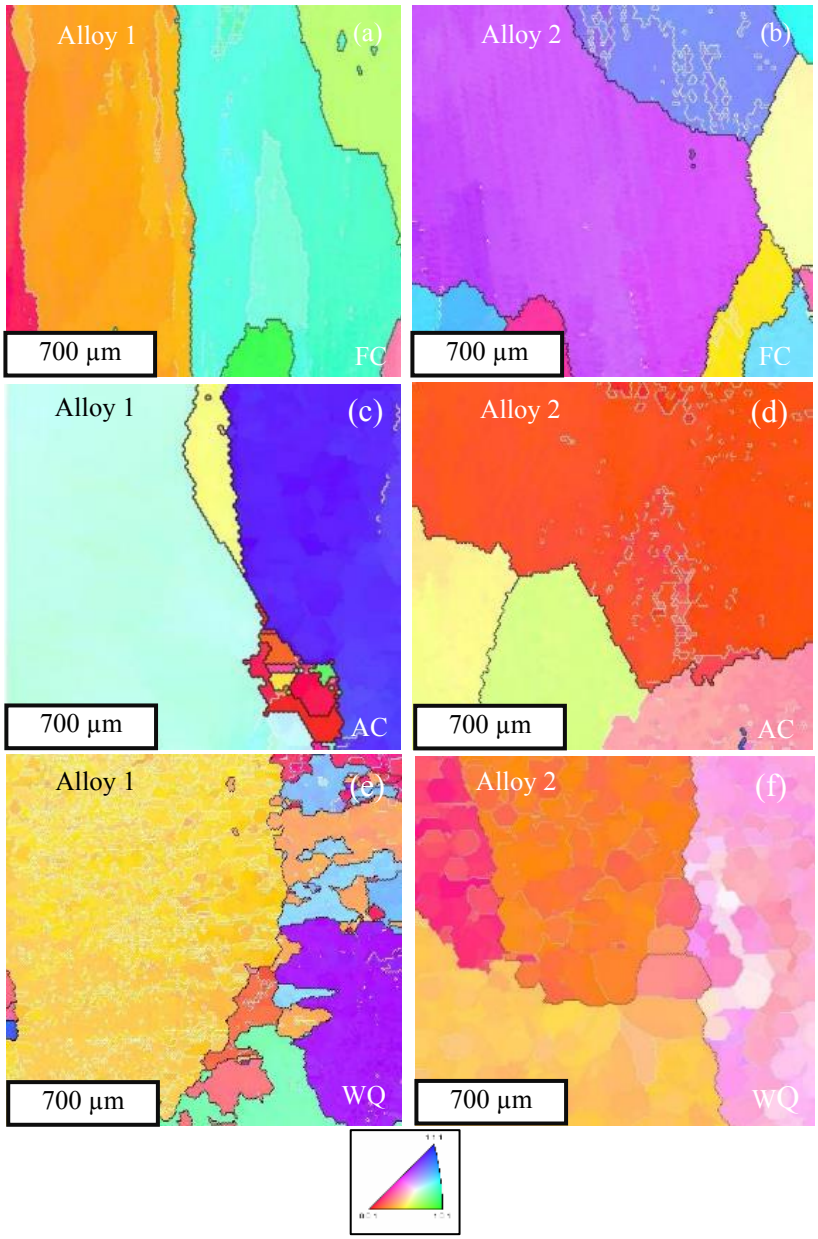

Fig. 5. IPF EBSD micrographs of studied CCAs, FC; furnace cooled, AC; air cooled, WQ; water quenched. Color coding is according to the standard triangle shown in the bottom of the figure.

[DOI: 10.22068/ijmse.17.4.130]

SEM analysis also showed a very low density of precipitates at grain interiors and boundaries of air and furnace cooled Alloy 1 (Figs. 6 (c) and (e)). However, this behaviour was not observed in water quenched sample (Fig. 6 (g)). Although it was outside the scope of this investigation to determine the nature of precipitates, the results suggested a possible precipitation in Alloy 1 during slow cooling. Other researchers also have reported the possibility of precipitation in equiatomic CoCrFeMnNi HEA during annealing at a similar range of temperature [17, 18, 36].

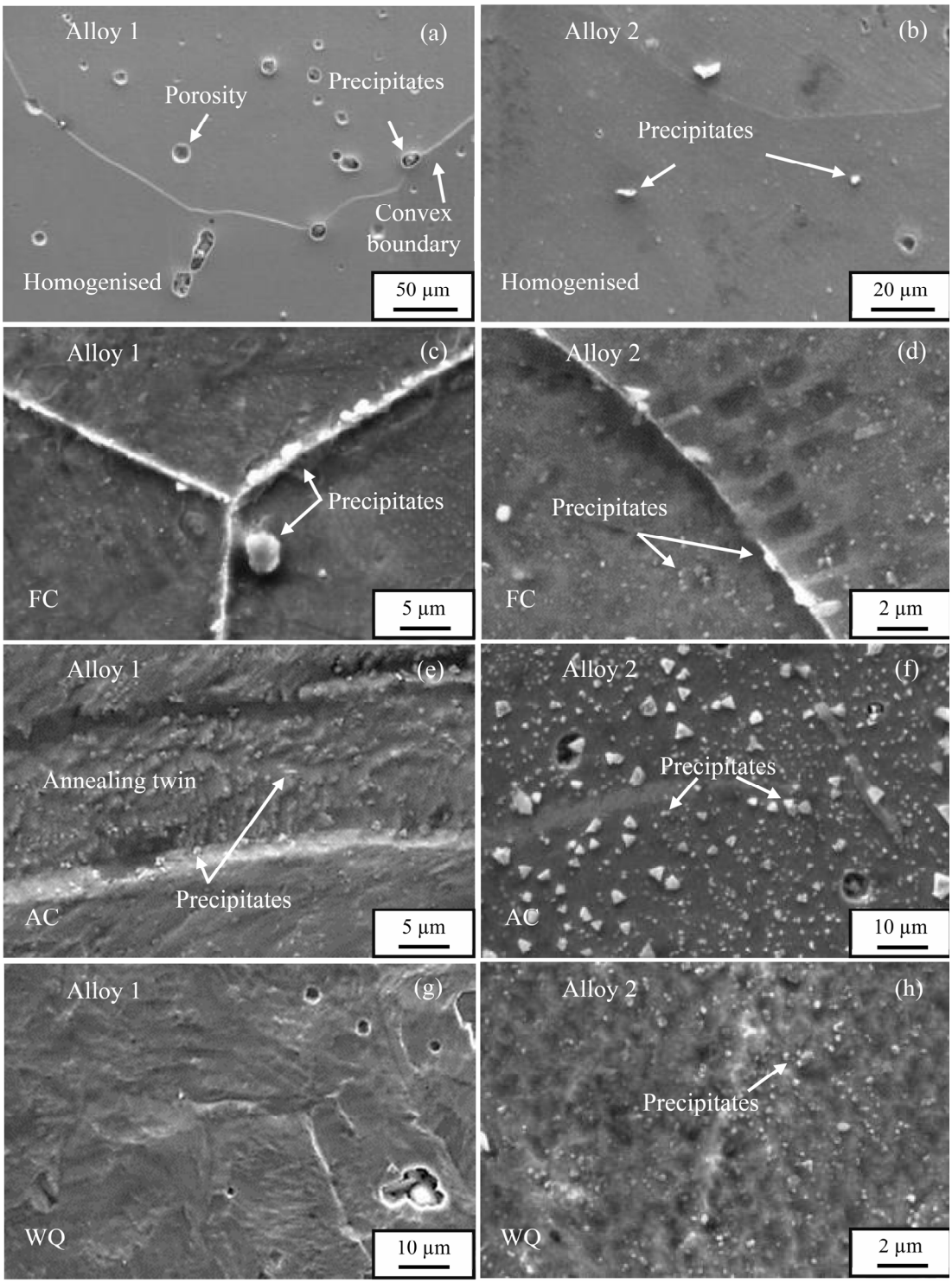

Fig. 6. Selected SEM micrographs of studied alloys, before and after annealing.

[DOI: 10.22068/ijmse.17.4.130]

In Alloy 2, precipitation was observed after annealing (Fig. 6). Generally, SEM analysis suggested a heterogenous distribution of precipitates in the microstructure of all samples. Nevertheless, no meaningful trend was observed in the size distribution and density of precipitates among the water quenched, air cooled and furnace cooled samples.

Qualitative SEM-WDX of matrix did not show any significant segregation of alloying elements in the matrix of studied alloys. Further qualitative microanalysis of samples demonstrated the presence of Mn-rich particles in the microstructure of both alloys, while Nb-rich precipitates were only observed in Alloy 2 (Fig. 6). Of particular note was that precipitates could significantly pin the grain boundaries, suggesting a possible inhibition of grain boundary migration during homogenisation and subsequent annealing (Figs. 3 and 6). This behaviour was also reported by Chen et al. for equiatomic CoCrFeMnNi HEA [37]. They suggested that Mn-Cr oxides can hinder the migration of grain boundaries. However, further investigations are suggested as future work to shed light on the concentration of different alloying elements in precipitates and matrix.

3.2. Crystal Structure Analysis

Fig. 7 shows XRD pattern of studied alloys. The XRD results showed a single-phase FCC crystal structure in all samples, regardless of cooling rate after annealing. Thus, the annealing did not alter the crystal structure of studied alloys.

From the XRD analysis, it was also found that the lattice parameter of Alloy 1 was slightly smaller than Alloy 2 (Table 2 and Fig. 7). Note that this difference was observed in all samples before and after annealing and in all cooling conditions.

Table 2 compares the approximated dislocation density of studied samples. The results suggested that the quenching process raised the dislocation density of both alloys.

The results indicated insignificant variations in the peak intensity of XRD pattern in terms of cooling rate (Fig. 7). Note that the lattice distortion can reduce the crystallisation perfection and enhance the scattering effect which decreases peak intensity [38, 39]. However, the results suggested that the cooling conditions did not noticeably affect the lattice distortion of studied alloys.

Table 2. Lattice parameter and dislocation density

	Alloy 1				Alloy 2			
	Homogenised	Water quenched	Air cooled	Furnace cooled	Homogenised	Water quenched	Air cooled	Furnace cooled
Lattice parameter (nm)	0.3589±0.0001	0.3587±0.0006	0.3590±0.0007	0.3590±0.0009	0.3615±0.0005	0.3616±0.0001	0.3617±0.0009	0.3611±0.0002
Dislocation density (10^{14} m^{-2})	0.27	4.08	3.48	3.80	1.61	5.68	2.11	3.50

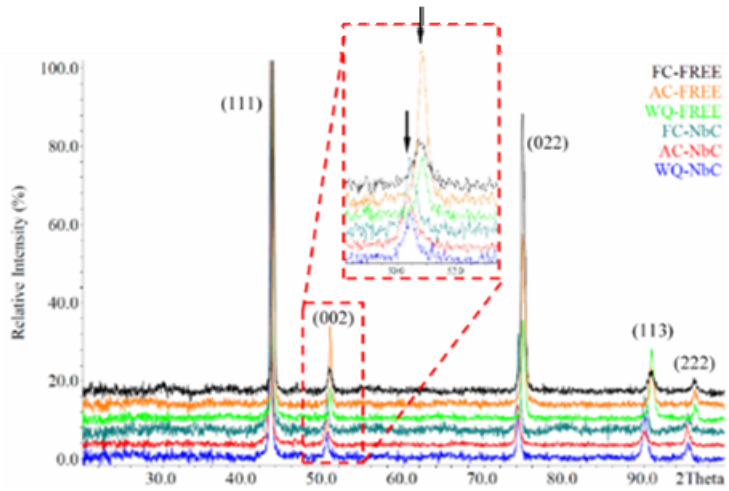

Fig. 7. XRD spectra, showing a FCC crystal structure in all samples, FC; furnace cooled, AC; air cooled, WQ; water quenched.

[DOI: 10.22068/ijmse.17.4.130]

3.3. Hardness

Fig. 8 highlights the hardness variations of studied alloys, related to different cooling conditions. The hardness of Alloy 2 was relatively higher than Alloy 1 in all conditions. It was also found that water quenching, air cooling and furnace cooling marginally influenced the results. Despite very slight fluctuation in the average hardness of samples, the results suggested that the studied alloys were not sensitive to cooling conditions after annealing.

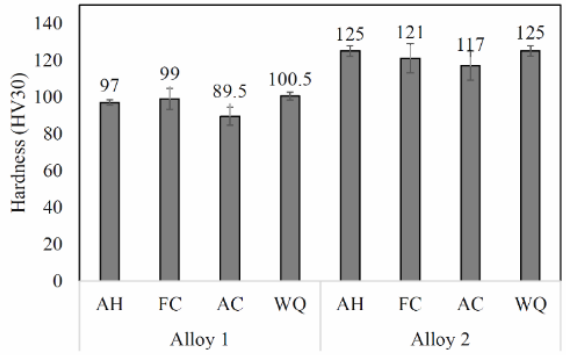

Fig. 8. Hardness variations in terms of cooling rate, AH; as-homogenised, FC; furnace cooled, AC; air cooled, WQ; water quenched.

4. DISCUSSION

4.1. Microstructure

Microscopy observations and XRD analysis showed a FCC crystalline structure matrix in all samples of studied alloys. It was clear that the cooling rate during annealing did not influence the crystalline structure of matrix of studied alloys. Further details of cooling rate effect on the microstructure will be discussed next.

In Alloy 1, microscopy observations showed the formation of fine grains at very small regions in the centre of water quenched and air-cooled samples (Figs. 3 and 5). This indicated that recrystallisation locally occurred, while the lack of driving force near the surface of sample deterred recrystallisation. Other researchers also have reported the possibility of quenching induced recrystallisation during annealing process for un-cold worked alloys [40, 41]. It is thought that the driving force for the recrystallisation resulted from different cooling rates from the surface to the core of samples during the cooling stage of homogenisation (Fig. 1). FEM analysis also evidenced that thermal contraction of surface during rapid air-cooling exerted inward forces which might promote crystalline defects inside samples (Fig. 2). This agrees with XRD results that also suggested the presence of dislocations inside the homogenised samples of both alloys (Table 2). However, an investigation into the role of quenching process on recrystallisation is currently an active topic for further studies.

The microscopy analysis indicated no recrystallisation in Alloy 2 after annealing (Fig. 3). It was clear that different stoichiometry of principal elements and also the Nb-C addition significantly retarded recrystallisation in Alloy 1. The recovery and rearrangement of dislocations encouraged sub-structure formation [42]. However, rapid cooling during water quenching minimised the possible recovery and annihilation of observed low-angle-boundaries or sub-structure (Fig. 5).

A careful SEM analysis of samples suggested a non-uniform distribution of precipitates in Alloy 2 (e.g. Fig. 6). This might mainly inherit from the as-cast microstructure of studied alloys. In a wider sense, a heterogenous distribution of crystalline defects and micro-segregation of alloying elements could encourage a heterogenous precipitation. This is consistent with other reports in the literature about the precipitation behaviour in CCAs/HEAs, despite their sluggish diffusion coefficient [43, 44].

4.2. Hardness

To interpret the hardness results, common hardening mechanisms were taken into consideration, including, grain size refinement, solid solution hardening, precipitation hardening and crystalline defects effect [10, 45-47].

Hardness analyses showed that the hardness of Alloy 2 was generally higher than Alloy 1 (Fig. 8). According to microscopy observations and XRD-analysis, the observed precipitation and solid solution hardening of alloying elements were considered as the main hardening mechanisms. This is similar to other reports in the literature [8, 23, 24, 48], suggesting that different stoichiometries of principal alloying elements and also Nb-C addition were mainly responsible for the hardening of Alloy 2 compared to Alloy 1.

The hardness results also demonstrated a rather similar level of hardness among water quenched,

[DOI: 10.22068/ijmse.17.4.130]

air cooled and furnace cooled samples in both alloys. In water quenched and air cooled Alloy 1, hardness measurements showed insignificant variations from un-recrystallised to recrystallised regions of the sample (Fig. 3). These results suggested that the hardness of Alloy 1 was not influenced by the finer grain size of recrystallised region. In spite of microstructural variations, it can be concluded that the solid solution hardening has the main contribution in hardness for the Alloy 1.

Similarly, the hardness of Alloy 2 was not significantly affected by cooling rate after annealing, although a heterogenous precipitation was observed. Our results suggested that the solid solution hardening was primarily responsible for the strength of studied alloy and the precipitation might not effectively contribute to hardening.

5. CONCLUSION

The effect of cooling rate on the microstructure and hardness of Alloy 1 and Alloy 2 during annealing was studied. The main conclusions can be summarised as follows:

1. Microscopy and XRD results showed a FCC crystal structure matrix in both alloys after annealing, regardless of cooling rate. Clearly, the cooling rate did not alter the high entropy matrix of both alloys.
2. Microscopy observations indicated grain coarsening during furnace and air cooling in Alloy 1, while no variation was observed in the grain size of Alloy 2.
3. An extensive precipitation was observed in Alloy 2 after annealing, while a very low density of precipitates appeared in Alloy 2 after only air and furnace cooling.
4. From the hardness analysis, it was found that the applied cooling rates did not generally influence the hardness of studied alloys, despite observed microstructural variations. The results suggested that the hardness is mainly controlled by solid solution strengthening.
5. Rapid cooling during homogenisation induced recrystallisation during subsequent annealing process for un-cold worked Alloy 1. However, further investigations would be required to better understand this phenomenon.

AUTHOR CONTRIBUTION

Erfan Abbasi designed and carried out experimental research, FEM and data analyses and wrote the paper and revisions. Kamran Dehghani supervised the project and Seyed Vahid Sajadifar and Thomas Niendorf performed EBSD analysis.

REFERENCES

1. Ye, Y. F., Wang, Q., Lu, J., Liu, C. T. and Yang, Y., "High-entropy Alloy: Challenges and Prospects." Mater. Today, 2016, 19, 349-362.
2. Lyu, Z., Lee, C., Wang, S. Y., Fan, X., Yeh, J. W. and Liaw, P. K., "Effects of Constituent Elements and Fabrication Methods on Mechanical Behavior of High-Entropy Alloys: A Review." Metall. Mater. Trans. A, 2018, 50, 1-28.
3. Abbasi, E. and Dehghani, K., "Hot Tensile Properties of CoCrFeMnNi (NbC) Compositionally Complex Alloys." Mater. Sci. Eng. A, 2020, 772 138771.
4. Manzoni, A. M. and Glatzel, U., "New Multiphase Compositionally Complex Alloys Driven by the High Entropy Alloy Approach." Mater. Charact., 2019, 147, 512-532.
5. Miracle, D. B. and Senkov, O. N., "A Critical Review of High Entropy Alloys and Related Concepts." Acta Mater., 2017, 122, 448-511.
6. Li, Z., Pradeep, K. G., Deng, Y., Raabe, D. and Tasan, C. C., "Metastable High-entropy Dual-phase Alloys Overcome the Strength–ductility Trade-off." Nature, 2016, 534, 227-230.
7. Gorsse, S., Couziniéc, J. Ph. and Miracle, D. B., "From High-entropy Alloys to Complex Concentrated Alloys." C. R. Phys., 2018, 19, 721-736.
8. Abbasi, E. and Dehghani, K., "Phase Prediction and Microstructure of Centrifugally Cast Non-equiatomic Co-Cr-Fe-Mn-Ni(Nb,C) High Entropy Alloys." J. Alloys Compd., 2019, 783, 292-299.
9. Guo, S., Ng, C., Lu, J. and Liu, C. T., "Effect of Valence Electron Concentration on Stability of FCC or BCC Phase in High Entropy Alloys." J. Appl. Phys., 2011, 103505.

[DOI: 10.22068/ijmse.17.4.130]

10. LaRosa, C. R., Shih, M., Varvenne, C. and Ghazisaeidi, M., "Solid Solution Strengthening Theories of High-entropy Alloys." Mater. Charact., 2019, 151, 310-317.
11. Totten, G. E., Bates, C. E. and Clinton, N. A., Handbook of Quenchants and Quenching Technology, ASM International, Oxford, UK, 1993.
12. Verlinden, B., Driver, J., Samajdar, I. and Doherty, R., Thermo-Mechanical Processing of Metallic Materials, Oxford, UK, 2007.
13. Xu, X. D., Guo, S., Nieh, T. G., Liu, C. T., Hirata, A. and Chen, M. W., "Effects of Mixing Enthalpy and Cooling Rate on Phase Formation of Al x CoCrCuFeNi High Entropy Alloys." Mater., 2019, 6, 100292.
14. Ma, L., Li, C., Jiang, Y., Zhou, J., Wang, L., Wang, F., Cao, T. and Xue, Y., "Cooling Rate-dependent Microstructure and Mechanical Properties of AlxSi0.2CrFeCoNiCu1-x High Entropy Alloys." J. Alloys Compd., 2017, 694, 61-67.
15. Molnár, D., Vida, A., Huang, S. and Chinh, N. Q., "The Effect of Cooling Rate on the Microstructure and Mechanical Properties of NiCoFeCrGa High Entropy Alloy." J. Mater. Sci., 2019, 54, 5074–5082.
16. Wei, R., Sun, H., Chen, C., Han, Z. and Li, F., "Effect of Cooling Rate on the Phase Structure and Magnetic Properties of Fe26.7Co28.5Ni28.5Si4.6B8.7P3 High Entropy Alloy." J. Magn. Magn. Mater., 2017, 435, 184-186.
17. Laplanche, G., Berglund, S., Reinhart, C., Kostka, A., Fox, F., and George, E. P., "Phase Stability and Kinetics of s-phase Precipitation in CrMnFeCoNi High Entropy Alloys." Acta Mater., 2018, 161, 338-351.
18. Pickering, E. J. and Jones, H. G., "High-entropy Alloys: A Critical Assessment of their Founding Principles and Future Prospects." Int. Mater. Rev., 2016, 61, 183-202.
19. He, J. Y., Wang, H., Wu, Y., Liu, X. J., Nieh, T. G. and Lu, Z. P., "High-temperature plastic flow of a precipitation-hardened FeCoNiCr high entropy alloy." Mater. Sci. Eng. A, 2017, 686, 34-40.
20. Abbasi, E., "Thermomechanical Processing of CoCrFeMnNi and CoCrFeMnNi(NbC) High Entropy Alloys." Amirkabir University of Technology, Tehran, Iran, 2018.
21. Pickering, E. J., Muñoz-Moreno, R., Stone, H. J. and Jones, N. G., "Precipitation in the Equiatomic High-entropy Alloy CrMnFeCoNi." Scr. Mater., 2016, 113, 106-109.
22. Otto, F., Dlouhy, A., Somsen, Ch., Bei, H., Eggeler, G. and George, E. P., "The Influences of Temperature and Microstructure on the Tensile Properties of a CoCrFeMnNi High-entropy Alloy." Acta Mater., 2013, 61, 5743–5755.
23. Ma, D., Yao, M., Pradeep, K. G., Tasan, C. C., Springer, H. and Raabe, D., "Phase Stability of Non-equiatomic CoCrFeMnNi High Entropy Alloys." Acta Mater., 2015, 98, 288–296.
24. Abbasi, E. and Dehghani, K., "Effect of Nb-C Addition on the Microstructure and Mechanical Properties of CoCrFeMnNi High Entropy Alloys during Homogenisation." Mater. Sci. Eng. A, 2019, 753, 224-231.
25. Haas, S., Mosbacher, M., Senkov, O. N., Feuerbacher, M., Freudenberger, J., Gezgin, S., Völkl, R. and Glatzel, U., "Entropy Determination of Single-Phase High Entropy Alloys with Different Crystal Structures over a Wide Temperature Range." Entropy, 2018, 654, e20090654.
26. Laplanche, G., Gadaud, P., Horst, O., Otto, F., Eggeler, G. and George, E. P., "Temperature Dependencies of the Elastic Moduli and Thermal Expansion Coefficient of an Equiatomic, Single-phase CoCrFeMnNi High-entropy Alloy." J. Alloys Compd., 2015, 623, 348–353.
27. Jin, K., Sales, B. C., Stocks, G. M., Samolyuk, G. D., Daene, M., Weber, W. J., Zhang, Y. and Bei, H., "Tailoring the Physical Properties of Ni-based Single-phase Equiatomic Alloys by Modifying the Chemical Complexity." Sci. Rep., 2016, 6, 20159.
28. Tirunilai, A. S., Sas, J., Weiss, K. P., Chen, H., Szabó, D. V., Schlabach, S., Haas, S., Geissler, D., Freudenberger, J., Heilmaier, M. and Kauffmann, A., "Peculiarities of Deformation of CoCrFeMnNi at Cryogenic Temperatures." J. Mater. Res., 2018, 33, 3287-3300.

[DOI: 10.22068/ijmse.17.4.130]

29. Bhattacharjee, P. P., Sathiaraj, G. D., Zaid, M., Gatti, J. R., Lee, Ch., Tsai, Ch. W. and Yeh, J. W., "Microstructure and Texture Evolution during Annealing of Equiatomic CoCrFeMnNi High-entropy Alloy." J. Alloys Compd., 2014, 587, 544-552.
30. Abbasi, E., Luo, Q. and Owens, D., "A Comparison of Microstructure and Mechanical Properties of Low-Alloy-Medium-Carbon Steels after Quench-hardening." Mater. Sci. Eng. A, 2018, 725, 65–75.
31. He, J. Y., Zhu, C., Zhou, D. Q., Liu, W. H., Nieh, T. G. and Lu, Z. P., "Steady State Flow of the FeCoNiCrMn High Entropy Alloy at Elevated Temperatures." Intermetallics, 2014, 55, 9-14.
32. Cheng, H., Wang, H. Y., Xie, Y. C., Tang, Q. H. and Dai, P. Q., "Controllable Fabrication of a Carbide Containing FeCoCrNiMn High-entropy Alloy: Microstructure and Mechanical Properties." Mater. Sci. Technol., 2017, 33, 2032-2039.
33. Totten, G. E., Quenching and Distortion Control, Ohio, USA, ASM International, 1993.
34. Totten, F., Howes, M. and Inoue, T., Handbook of Residual Stressand Deformation of Steel, Ohio, USA, ASM International, 2002.
35. Canale, L. C. F. and Narazaki, M., Quenching and Cooling, Residual Stress and Distortion Control, USA, ASTM International, 2010.
36. Ye, F., Jiao, Z. and Yang, Y., "Effect of Medium Temperature Precipitation Phase and Mn Element Diffusion Mechanism on High Temperature Oxidation Process of Repair and Remanufacture CoCrFeMnNi High-entropy Alloy Cladding." Mater. Res. Express, 2019, 6, 056521.
37. Chen, B. R., Yeh. A. C. and Yeh, J. W., "Effect of One-step Recrystallization on the Grain Boundary Evolution of CoCrFeMnNi High Entropy Alloy and Its Subsystems." Sci. Rep., 2016, 6, 22306.
38. Yeh, J. W., Chang, S. Y., Hong, Y. D., Chen, S. K. and Lin, S. J., "Anomalous Decrease in X-ray Diffraction Intensities of Cu–Ni–Al–Co–Cr–Fe–Si Alloy Systems with Multi-principal Elements." Mater. Chem. Phys., 2007, 103, 41-46.
39. Guo, W., Dmowski, W., Noh, J. Y., Rack, P., Liaw, P. K. and Egami, T., "Local Atomic Structure of a High-Entropy Alloy: An X-Ray and Neutron Scattering Study." Metall. Mater. Trans. A, 2012, 44, 1994–1997.
40. Xu, X. L. and Liu, F., "Crystal Growth Due to Recrystallization upon Annealing Rapid Solidification Microstructures of Depply Undercooled Single Phase Alloys Quenched before Recalescence." Cryst. Growth Des., 2014, 14, 2110-2114.
41. Xu, X., Hou, H., Zhao. Y. and Liu, F., "Preparation of Bulk Crystallite Alloys by Rapid Quenching of Bulk Undercooled Melts." Mater. Sci. Technol., 2018, 34, 79-85.
42. Humphreys, F. J. and Hatherly, M., Recrystallization and Related Annealing Phenomena, Second ed., Oxford, UK, 2004.
43. Jones, N. G., Christofidou, K. A. and Stone, H. J., "Rapid Precipitation in an Al0.5CrFeCoNiCu High Entropy Alloy." Mater. Sci. Technol., 2015, 31, 1171-1177.
44. Wei, S., He, F. and Tasan, C. C., "Metastability in High-entropy Alloys: A Review." Mater. Res. Soc., 2018, 33, 2924-2937.
45. Varvenne, C., Luque, A. and Curtin, W. A., "Theory of Strengthening in FCC High Entropy Alloys." Acta Mater., 2016, 118, 164-176.
46. Gladman, T., "Precipitation Hardening in Metals." Mater. Sci. Technol., 1999, 15, 30-36.
47. Sun, S. J., Tian, Y. Z., Lin, H. R., Dong, X. G., Wang, Y. H., Zhang, Z. J. and Zhang, Z. F., "Enhanced Strength and Ductility of Bulk CoCrFeMnNi High Entropy Alloy Having Fully Recrystallized Ultrafine Grained Structure." Mater. Des., 2017, 133, 122-127.
48. Gao, N., Lu, D. H., Zhao, Y. Y., Liu, X. W., Liu, G. H., Wu, Y., Liu, G., Fan, Z. T., Lu, Z. P. and George, E. P., "Strengthening of a CrMnFeCoNi High-entropy Alloy by Carbide Precipitation." J. Alloys Compd., 2019, 792, 1028-1035.

[DOI: 10.22068/ijmse.17.4.130]